Granular experiments of thrust wedges: Insights relevant to methane hydrate exploration at the Nankai accretionary prism

AUTHOR(S):

Yamada, Yasuhiro; Baba, Kei; Miyakawa, Ayumu; Matsuoka, Toshifumi

CITATION:

Yamada, Yasuhiro ...[et al]. Granular experiments of thrust wedges: Insights relevant to methane hydrate exploration at the Nankai accretionary prism. Marine and Petroleum Geology 2014, 51: 34-48

ISSUE DATE:

2014-03

URL:

http://hdl.handle.net/2433/180086

Marine and Petroleum Geology 51 (2014) 34–48

Contents lists available at ScienceDirect

Marine and Petroleum Geology

journal homepage: www.elsevier.com/locate/marpetgeo

Granular experiments of thrust wedges: Insights relevant to methane hydrate exploration at the Nankai accretionary prism☆

Yasuhiro Yamada [a,*], Kei Baba [b], Ayumu Miyakawa [c], Toshifumi Matsuoka [a]

[a] Department of Earth Resources Engineering, Kyoto University, Katsura, Nishikyo, Kyoto 615-8540, Japan
[b] Exploration Department, Japan Oil, Gas and Metals National Corporation (JOGMEC), 2-10-1 Toranomon, Minato, Tokyo 105-0001, Japan
[c] Geological Survey of Japan/AIST, AIST Tsukuba Central 7, Higashi-1-1-1, Tsukuba, Ibaraki 305-8567, Japan

ARTICLE INFO

Article history:
Received 17 August 2012
Received in revised form
11 November 2013
Accepted 13 November 2013
Available online 22 November 2013

Keywords:
Methane hydrates
Accretionary prism
Subduction margin
Analog model
Digital image correlation
Distinct element method

ABSTRACT

The accumulation mechanism of methane hydrates has been a central issue in previous hydrate research regarding the Nankai accretionary prism, southwest of Japan. Expulsion of formation fluids is significant during the prism accretion process, and the migration of these methane-bearing fluids exerts a strong control on the accumulation of hydrates. Two types of fluid pathways, inter-granular porosity and faults, need to be evaluated to understand hydrate accumulation. Fluid migration along faults can be partly modeled by examining faulting activity. Our study modeled the accretion process by using two granular methods that approximated the geologic body as an assemblage of particles: (1) analog experiments using granular materials, and (2) a numerical simulation based on the distinct element method. The analog experiments closely reproduced the prism geometry observed in seismic profiles across the Nankai accretionary prism. Digital image correlation analysis indicated that the frontal thrust is generally active but older structures are also frequently reactivated. The numerical simulations produced prism geometries similar to those of the analog experiments. The velocity distributions of the particles showed evidence of episodic faulting and reactivation, but the internal stress field exhibited little change in the deeper part of the prism during deformation. The frequent and substantial changes in fault activity displayed by the models indicate episodic fluid flow along fault surfaces. Active frontal thrusting suggests that formation fluids generally migrate from deep within the prism to the deformation front, but may move along reactivated older faults. Inter-granular permeability also fluctuates, as it is controlled by temporal and spatial variations in the internal stress field. However, fluid flow is likely to be relatively stable in the deeper segment of the prism.

1. Fluid flow and methane hydrates in accretionary prisms: an introduction

Vast quantities of methane hydrates are present in accretionary prisms around the world (Collett, 2002). The distribution of hydrates has been examined through the regional development of bottom simulating reflections (BSRs) on seismic profiles (e.g., Aoki et al., 1983; Minshull and White, 1989; Davis et al., 1990; Ferguson et al., 1993; Delisle et al., 1998; Ashi et al., 2002; Baba and Yamada, 2004). Allison and Boswell (2007) reported an estimated 400×10^6 trillion cubic feet (TCF) of methane gas in hydrates worldwide, which is at least 2–10 times greater than the confirmed conventional natural-gas reserves. Industrial and scientific drilling projects have confirmed the presence of methane hydrates in accretionary prisms in the Middle American Trench (Kvenvolden and McDonald, 1985), offshore Costa Rica (Shipboard Scientific Party Site 1041, 1997), the Cascadian margin, USA (Tréhu et al., 2003; Expedition 311 Scientists, 2005), and the Nankai Trough (Taira et al., 1992; Matsumoto, 2002; Tsuji et al., 2005; Kinoshita et al., 2008).

These studies have revealed many uncertainties regarding methane hydrates that require further examination. For example, although the existence of methane hydrates in accretionary prisms has been confirmed at several locations, the occurrence and accumulation of methane hydrate deposits are not fully understood. A recent geophysical investigation showed that the characteristics of BSRs in seismic profiles are strongly dependent on the method of data acquisition, in particular the type of seismic source used

* Corresponding author. Tel.: +81 75 383 3204; fax: +81 75 383 3203.
E-mail addresses: yamada@earth.kumst.kyoto-u.ac.jp (Y. Yamada), baba-kei@jogmec.go.jp (K. Baba), miyakawa-a@aist.go.jp (A. Miyakawa), matsuoka@earth.kumst.kyoto-u.ac.jp (T. Matsuoka).

0264-8172/$ – see front matter © 2013 The Authors. Published by Elsevier Ltd. All rights reserved.
http://dx.doi.org/10.1016/j.marpetgeo.2013.11.008

(Kamei et al., 2005). Our understanding of the rock physics of hydrate reservoirs is still relatively simple, with a focus on the microscale (e.g., Dvorkin et al., 2000), though efforts to measure flow velocities have been undertaken in a laboratory setting (e.g., Priest et al., 2005; Yun et al., 2005). Accurate methods for the detection of hydrates and evaluation of their regional volumes have not been established to date, other than that used in a study in the eastern Nankai area (Japan Oil, Gas and Metals National Corporation (JOGMEC), 2011), as detailed below.

Depressurization appears promising as a production method for methane gas from hydrates. This follows significant success at the Mallik test site for continental natural-gas hydrates in the Mackenzie Delta in the northwestern Canadian Arctic (Research Consortium for Methane Hydrate Resources in Japan, 2008). The methods for production of offshore hydrates are, however, still being examined exclusively in laboratories, except for one offshore experiment in the Nankai Trough (JOGMEC, 2011).

Hydrate research has clarified several aspects of the formation and accumulation of methane hydrates. The formation of methane hydrates is primarily controlled by the chemical conditions of hydrate stability and methane solubility in the formation water (e.g., Claypool and Kaplan, 1974; Pecher et al., 1998; Clennell et al., 2000). The gas hydrate stability zone (GHSZ) in ocean-floor sediments is located between the ocean floor and the maximum depth below the ocean floor at which gas hydrates are stable, as defined by temperature and pressure. In a typical accretionary prism, where heat flow is usually low (e.g., Yamano et al., 1982; Ashi et al., 2002), the base of the GHSZ is a few hundred meters below the ocean floor. As accretionary prisms are tectonically active, pressure conditions are not always static, meaning that the depth of the base of the stability zone also fluctuates. For example, when sediments are uplifted by thrust movement, the base of the stability zone migrates upward due to the reduction in pore fluid pressure. This upward migration causes dissociation of hydrates at the former base of the GHSZ, and subsequent upward migration of the dissociated gas. The migrated dissociated gas then re-forms gas hydrates at the base of the new stability zone—this may be the mechanism that causes methane hydrate concentration near the base of the stability zone (e.g., Bangs et al., 2005). Actual methane hydrates are distributed in the gas hydrate occurrence zone (GHOZ) where the concentration of methane exceeds its solubility in the formation water (Tréhu et al., 2006). This occurrence zone generally occupies the lower–middle part of the stability zone.

Methane can be classified as biogenic or thermogenic, based on the processes by which it formed. Biogenic methane is generated by the biological activity of methane-producing bacteria in sediments at shallow depths below the ocean floor (Claypool and Kaplan, 1974). The generation of thermogenic methane usually occurs in deeply buried sediments, typically greater than 2 km below the ocean floor (Tréhu et al., 2006), and may be the result of the same processes that produce hydrocarbons in sedimentary basins (Hyndman and Davis, 1992). Although the content of organic carbon in the accreting sediments is sometimes less than 1% (e.g., Nankai; Taira et al., 1992; Waseda, 1998), BSRs can still be observed in such regions, suggesting some uncertainty in the generation mechanism of methane at convergent margins.

The two modes of methane generation suggest that the distribution patterns of biogenic and thermogenic methane hydrates are likely to be significantly different. Microbial methane can be generated wherever sediments contain organic carbon (Davie and Buffett, 2001). The average concentration of biogenic methane hydrates is generally equivalent to a small percentage of the total porosity (e.g., Lorenson, 2000; Tréhu et al., 2004), and such hydrates tend to accumulate near the base of the hydrate occurrence zone. In contrast, thermogenic methane migrates from deeply buried sediments along fluid pathways, driven by the advection of formation fluids. Thermogenic methane may be periodically expelled from the formation zone, and subsequently migrates to the GHOZ. Therefore, thermogenic methane hydrates are frequently concentrated in faults and high-permeability layers that form the migration pathways for the fluid. The concentration of hydrates in the GHOZ increases over time, as long as the 'petroleum system' of thermogenic methane generation and migration is maintained. The concentration of thermogenic methane hydrate is generally much higher than that of sparsely distributed biogenic methane hydrates. We suggest that these concentrated thermogenic hydrates are the best candidates for commercial methane hydrate exploration.

To clarify the accumulation mechanism of thermogenic methane hydrates in accretionary prisms, the migration of formation fluids needs to be examined in detail (Baba and Yamada, 2004). The fluid pathways in accretionary prisms can be classified into two types: migration through inter-granular pore spaces, and migration along faults (Fig. 1). Given that the accreted sediments are weakly consolidated, inter-granular porosity is expected to be extremely high (e.g., 61% recorded by Dugan and Flemings (2000)). This is particularly significant in shallower sediments where fluid flows through inter-granular pore spaces. This type of fluid flow, called 'diffusive flow' (Baba and Yamada, 2004), is primarily controlled by the stress field, including the overburden pressure, which affects the volume and geometry of the inter-granular pore space. Fluid flow along faults, termed 'focused flow' (Baba and Yamada, 2004), plays a more important role in deeper sediments, which are relatively consolidated and less permeable. The occurrence of focused fluid flow in accretionary prisms has been confirmed by isotope analysis, heat-flow measurements, and analyses of hydrates (e.g., Sample, 1996; Suess et al., 1999). Fluid flow in accretionary prisms is a combination of these two flow types (Fig. 1). In deeper parts of the prism, fluid expelled by the overburden pressure predominantly migrates along faults (focused flow). Most of the fluids then migrate to shallower horizons through inter-granular pore spaces (diffusive flow) to form hydrates in the occurrence zone.

Qualitative modeling of diffusive flow is possible through the use of conventional reservoir simulators, but no universal method has been established to model focused flow (Hickman et al., 1995; Wilkins and Naruk, 2007). Sibson (1990) proposed a model of focused flow in which fluid flow occurs along a fault surface coeval with fault displacement, driven by the hydromechanical behavior of the fault. This fault-valve model requires a large amount of high-

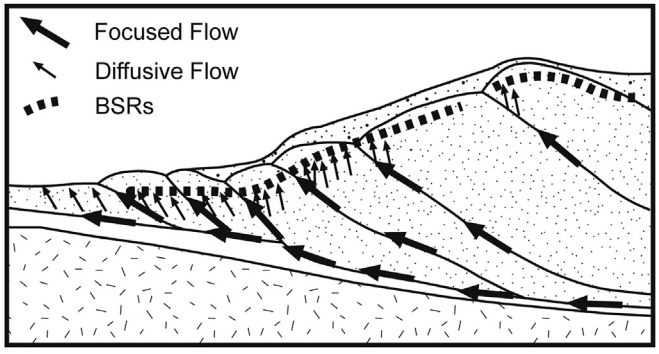

Figure 1. Model of fluid flow within an accretionary prism (after Baba and Yamada, 2004). The fluid pathways can be classified into two types: diffusive flow through inter-granular pore spaces, and focused flow along faults. The total fluid flow is the sum of these two types.

pressure fluid beneath a low-permeability seal during inter-seismic periods. Fluid is forced upward immediately after a faulting event as the seal is broken. An alternative model, established in the field of mining geology, suggests that impermeable barriers form along fault zones due to cementation and fracture healing. This is followed by episodic fracturing and subsequent enhancement of porosity and permeability during slippage events, producing intermittent fluctuations in fluid pressure (Sibson, 1992; Sleep and Blanpied, 1992; Byerlee, 1993). A third model, proposed by researchers in the field of geomechanics, states that hydraulically conductive fractures are critically stressed in the in situ stress environment (Barton et al., 1995; Finkbeiner et al., 1997; Wiprut and Zoback, 2000). This model can be successfully applied to crystalline basement rocks (Barton et al., 1995), but its applicability to unconsolidated sedimentary rocks is unclear (Wilkins and Naruk, 2007). Wilkins and Naruk (2007) argued that seismic slip causes transient dilation along the fault, which effectively enhances fluid migration, whereas aseismic slip does not significantly enhance fluid migration along the fault. According to this model, fault activity can be used to estimate the focused flow in prisms where dilation occurs along the fault.

This paper attempts to model the fluid flow in accretionary prisms for the purpose of methane hydrate exploration and production, and the model is applied to hydrates in the Nankai Trough area, southwest of Japan. We employed two methods in this study, both of which approximate the geologic body as an assemblage of particles: (1) analog experiments that use granular materials such as dry sand and microbeads, and (2) numerical simulations based on the distinct element method (DEM). Such simulation techniques are useful because the brittle deformation behavior of rocks can be suitably modeled by an assemblage of particles (McClay, 1990) while fulfilling the scaling theory of Hubbert (1937). As the timescales of the structural deformation and fluid flow differ significantly, detailed examinations of the deformation process over a short timescale are vital to construct models of fluid flow along faults. We examined fault activity during prism formation in detail, using a combination of analog models with image correlation and numerical results employing shorter time steps. We also examined dilation along the fault surface using these two techniques.

2. Nankai accretionary prism and methane hydrates

The Nankai accretionary prism has been the subject of much geoscience research, in fields such as structural geology (e.g., Taira et al., 1988; Henry et al., 2002; Ujiie et al., 2003), seismology (e.g., Ando, 1975; Hyndman et al., 1995; Tanioka and Satake, 2001), and methane hydrate exploration (e.g., Baba and Yamada, 2004; Tsuji et al., 2004; Matsushima, 2005; Fujii et al., 2008). At the Nankai Trough, the Philippine Sea Plate is subducting beneath the Eurasian Plate (Fig. 2a) at a rate of 4 cm/year in the direction of 310–315° (Seno et al., 1993). The incoming sediments upon the basaltic oceanic crust consist of hemipelagic mudstone and turbiditic alternations of sandstone and mudstone derived from the island arc. A décollement (the plate boundary) is clearly identifiable within the hemipelagic mudstone (Fig. 2b) as a reflection with reverse polarity (Moore et al., 1990; Bangs et al., 2004). This reflective characteristic is generally produced by a sharp drop in the acoustic impedance of sediments, which is well correlated with a rapid decrease in bulk density at the top of the underthrust sediments, as reported by ODP scientific drilling (Moore et al., 2001). The density decrease immediately beneath this horizon, without cementation in the sediments, suggests an elevation in the fluid pressure at the base of the décollement (Ujiie et al., 2003). The décollement horizon can also be traced in the undeformed regions seaward of the deformation front (Fig. 2b). Assuming that fluid sealing occurs along the décollement, the layer that forms the décollement may be predefined by the fluid permeability of incoming sediments prior to the initiation of displacement (Tsuji et al., 2005). These observations provide support for the argument that deformation at Nankai is strongly influenced by fluid flow (e.g., Le Pichon et al., 1987; Moore, 1989; Henry et al., 2002).

Methane hydrates (including those indicated by BSRs) in the Nankai Trough area are distributed in the forearc basin sediments and in the prism sediments, which are commonly deformed. Japan National Oil Corporation (JNOC) (1998) estimated the total volume of methane gas in the hydrates to be 1765 TCF based on the distribution of BSRs around the Japanese islands. Ashi et al. (2002) interpreted 2D seismic profiles and proposed several models for the production of BSRs in accretionary prisms. As discussed above, the key factor in the generation of strong BSRs is the process of hydrate recycling around the base of the hydrate stability zone (BHSZ), produced by a rise in the BHSZ due to tectonic uplift and erosion. Baba and Yamada (2004) also interpreted a dense 2D seismic dataset in the Nankai area, acquired for hydrocarbon exploration, and classified the BSRs into four major types: ridge, buried anticline, basin margin, and accretionary prism. All of these types are closely associated with methane migration to the BHSZ, thus emphasizing the significant role of formation fluids in methane hydrate accumulation.

JOGMEC conducted a drilling program for the exploration of methane hydrates in the forearc basin deposits at the eastern Nankai wedge, confirming the existence of hydrates in the intergranular pore spaces of turbidite sandstones (Matsumoto, 2002; Tsuji et al., 2004; Matsushima, 2005). Fujii et al. (2008) examined well data, combined with 2D and 3D seismic profiles, and estimated 40 TCF of in situ methane gas stored as hydrates in the eastern Nankai region. Scientific drilling in the neighboring Kumano Basin area confirmed the extensive development of hydrates in turbidite sandstones (Kinoshita et al., 2008). The hydrate reservoirs in these areas appear to be limited to particularly permeable segments of sandstones.

3. Methods

3.1. Geologic modeling of the Nankai accretionary prism

A reliable model of the Nankai accretionary prism must incorporate its characteristic features, including the detachment surface (décollement). Mechanical decoupling at the base of the décollement may be due to an elevation in fluid pressure (Ujiie et al., 2003), which reduces the stress normal to the décollement and therefore reduces friction. Cobbold et al. (2001) constructed an experimental apparatus that increased the fluid pressure in their thrust analog models, confirming that the increased pressure produced a decreased taper angle and widened fault spacing. These effects are similar to those noted in experiments that include a décollement with a lower internal friction coefficient; thus, low-friction materials may be used to approximate the effects of elevated fluid pressure (Yamada et al., 2006a). To produce the detachment surface in this study, we modeled sediments using granular materials with a low-friction layer.

To model the accretion process, we used a simple bulldozer style of horizontal shortening, which is widely used in previous studies (e.g., von Houne and Scholl, 1991). There are two methods that can be used when conducting these types of experiments: pushing a rigid backstop from the rear, or pulling a sheet from beneath the materials. Schreurs et al. (2006) conducted a series of benchmark analog experiments comparing the two kinematic shortening

methods, and found that the results were fundamentally the same, except for the boundary effects of side walls. In the present study, the latter method was used in analog experiments, and the former in numerical simulations (Fig. 3), to ensure simplicity in the modeling and to obtain higher-resolution results.

3.2. Analog experiments

Physical experimentation using analog materials is a useful technique to visualize the geometry and deformation processes of accretionary prisms (see Malavieille, 1984; Mulugeta, 1988; Colletta et al., 1991; Liu et al., 1992; Mulugeta and Koyi, 1992; Gutscher et al., 1996; Storti et al., 1997, 2000; also see Graveleau et al., 2012 for a thematic list of studies since 2000 that have employed experimental wedge models). In particular, experiments using dry sand can accurately model the typical deformation behavior of rock; i.e., an elastic–frictional plastic with strain-hardening preceding failure (at peak strength) followed by strain-softening until a dynamically constant shear load is reached (Lohrmann et al., 2003). Such granular materials are therefore widely used to simulate geological structures (see Appendix A of Cobbold and Castro, 1999 for a thematic list of 'sandbox' references published up to 1998; also see Koyi and Mancktelow, 2001; Yamada and McClay, 2003a,b, 2004; McClay, 2004; Yamada et al., 2005).

The apparatus for the experiment was an acrylic box of $25 \times 150 \times 50$ cm with a plastic sheet on the bottom (Fig. 3a). We layered granular materials on top of the sheet, which was then pulled by an electric motor at a constant speed of 1.67×10^{-3} cm/s through a gap between the fixed base and a fixed endwall. The model was shortened by a total of 50 cm. We used dry cohesionless quartz sand and glass microbeads as the granular materials. The quartz sand was sourced from Toyoura Beach (Japan), has an average grain size of 200 μm, and is a popular material for physical tests in civil engineering in Japan. The spherical glass microbeads used were approximately 50 μm in diameter, and are considered a suitable analog for weaker layers (e.g., Lohrmann et al., 2003; Yamada et al., 2004, 2006a). Our shearing tests showed that the internal frictional angles of the Toyoura sand and the microbeads were 34° and 25°, respectively, and both materials showed dilation (Yamada et al., 2006b). A series of ring shear tests on these materials confirmed these results and showed that the cohesion of the Toyoura sand and the microbeads are ca. 130 and 40 Pa, respectively. Sand was glued to the surface of the sheet to avoid unnecessary slip, and this base layer was displaced during the experiments.

The thickness of the undeformed sediments above the décollement surface at the Nankai Trough is 400–800 m along the seismic line shown in Figure 2b, and 600–800 m at the NanTroSEIZE drilling site (Kinoshita et al., 2008), approximately 200 km

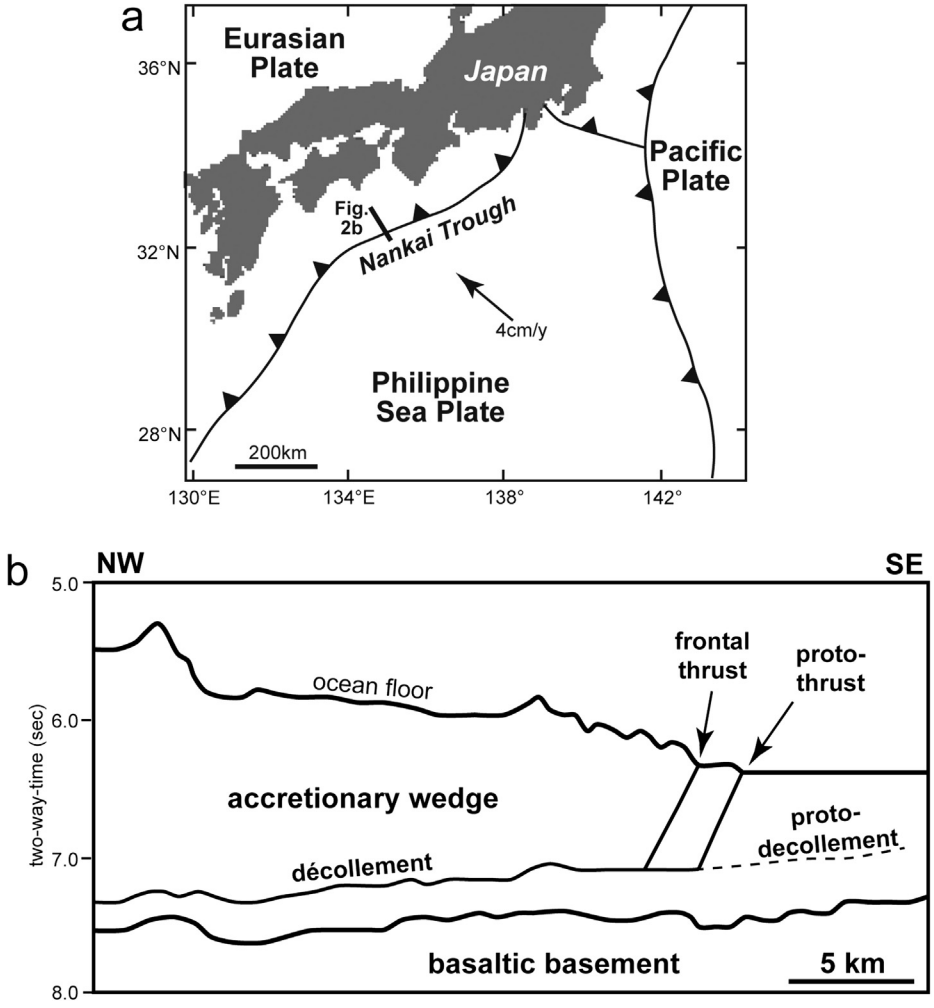

Figure 2. (a) Tectonic setting of the Nankai Trough and (b) line drawing of a seismic profile at the toe of the Nankai accretionary prism. The Nankai Trough is a convergent margin where the Philippine Sea Plate is subducting beneath southwestern Japan. The décollement is identified within the hemipelagic mudstone in the profile, and can be traced in the undeformed sequence as a 'proto-décollement' (Tsuji et al., 2005).

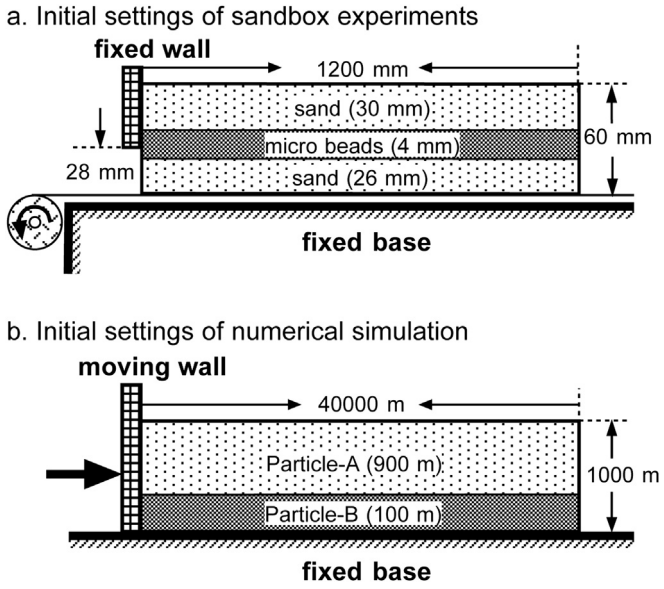

Figure 3. Initial setup of (a) analog experiments and (b) numerical simulation. To produce horizontal shortening, the materials were displaced relative to the fixed wall in the analog models, and a moving wall pushed the particles in the numerical models. The difference in the shortening kinematics has no significant impact on the results, according to Schreurs et al. (2006).

northeast of the seismic line. The material in the experiment was 3.0 cm thick, based on the thickness-to-length ratio of the natural accretionary prism, and the ratio of the length in the model to that in nature ranged from 3.8×10^{-5} to 7.5×10^{-5}. This value is within the range (10^{-4}–10^{-5}) for which scaled models using granular materials can be used to accurately model brittle deformation of the upper crust (McClay, 1990). The total length of horizontal shortening applied to the model corresponds to 6.7–13.0 km of shortening in the natural setting, equivalent to the amount of plate convergence over the past $1.7–3.4 \times 10^5$ years (Seno et al., 1993).

This study employed digital image correlation (DIC), which evaluates time-lapse digital photographs of the experiments and calculates the displacement field of the grains. The accuracy of the calculated displacement depends on the image region and the resolution of the digital camera (Wolf et al., 2003). In this study, the pixel size is 0.0971 mm. Assuming a theoretical resolution of displacement of one-fortieth of this pixel size for an interrogation window size of 32×32 pixels (La Vision, 2010), this results in a resolution of 2.43 μm. DIC data can also extract the stick–slip motions of each fault in analog experiments, with a scaling factor of 10^5–10^6 (Adam et al., 2005). The precise distributions of strain magnitude can then be derived using the calculated displacement field (Adam et al., 2005). This technique is commonly used for dynamic flow analysis and soil mechanics (e.g., Hryciw et al., 1996), but has also recently been applied to structural analog models (Wolf et al., 2003; Adam et al., 2005; Yamada et al., 2006a, 2010) and is now recognized as an excellent tool for analyzing results from such models. This study uses shear strain only rather than any other type of strain.

3.3. Numerical simulations

We performed numerical simulations using the DEM employing discrete circular elements (Cundall and Strack, 1979). In this method, linear elasticity (force–displacement law; Cundall and Strack, 1979) is incorporated through normal and shear forces at elemental contacts. Inter-element shear friction is determined by the normal force and a friction coefficient. The method consists of two steps in each calculation cycle (time step): evaluation of interaction forces for each element, and the movement of elements according to numerical integration, following Newton's equation of motion for the given external forces (Cundall and Strack, 1979). Each element is rigid against deformation, in such a way that volume change, including dilation, is accommodated by the inter-element porosity. This method can incorporate discontinuity surfaces without a priori information or parameters, which is the primary advantage of DEM over continuum methods such as finite element method (FEM). DEM is a relatively new technique but has been applied to the analysis of structural development processes (Saltzer and Pollard, 1992; Saltzer, 1993; Donze et al., 1994; Strayer and Suppe, 2002; Finch et al., 2003; Yamada et al., 2006a; Miyakawa et al., 2010). The software employed in this study is the commercial program PFC2D (ITASCA Corporation, Minneapolis, USA).

As DEM can only determine the parameters related to the contact points of the elements, compression-test simulations were necessary to measure the physical properties of the bulk element assemblage. We conducted a series of bi-axial compression tests for a number of parameter combinations, and found one particle type, particle-A, had an internal frictional angle of 35°, while another particle type, particle-B, had an internal frictional angle of 25°. These values correspond to those of the sand and microbeads, respectively, used in the analog experiments. The friction coefficient between the wall and the particles was the same as that of particle-A throughout this study. The negligible cohesion (ca. 40–130 Pa) of the analog modeling materials meant that initial cohesion and bonding between elements were not simulated. To avoid the formation of preferential weak planes in the initial arrangement of the element assemblage, we used a random variation for the diameter of each element in ranges of 12–30 m and 6–10 m for particle-A and particle-B, respectively.

The initial geometry of the particle assemblage was a $40{,}000 \times 1000$ m rectangle, with a thickness of 900 m of particle-A and 100 m of particle-B (Fig. 3b). A rigid wall pushed one side of the assemblage horizontally. There was no gap between the bottom of the moving wall and the fixed base. The displacement of 0.09 cm for each calculation cycle was determined, after a series of preliminary simulations, to be small enough to approximate the deformation as quasi-static. Using the simulation with these parameters required approximately 1.0×10^7 calculation steps to generate the equivalent horizontal shortening applied during the analog experiments.

4. Results of analog experiments

4.1. Deformation geometry and DIC strain

The experiments produced typical wedge geometries with a series of foreland-verging thrusts that propagated upward from the microbead layer (Fig. 4). Each thrust dips at 20°–35° and has an associated minor hinterland-verging backthrust. Each thrust–backthrust pair delineates a characteristic triangular pop-up structure (McClay, 2004). The surface slope of the wedge is 8°–9°, and the fault spacing of the frontal thrusts is approximately 9 cm at the deformation front, at which point the fixed backstop may have a small effect. Sand on the prism slope glided down into the toe of the prism and filled the trough. This caused thickness changes to the upper layers; i.e., thinning of the top sand layer (white layer in Fig. 4) and second sand layer (black layer) on the prism slope, and thickening in the trough (Fig. 4). These patterns are consistent with the typical development of accretionary wedges.

From the shear strain distributions analyzed by the DIC technique, the detailed activity of the faults can be recognized (Fig. 4).

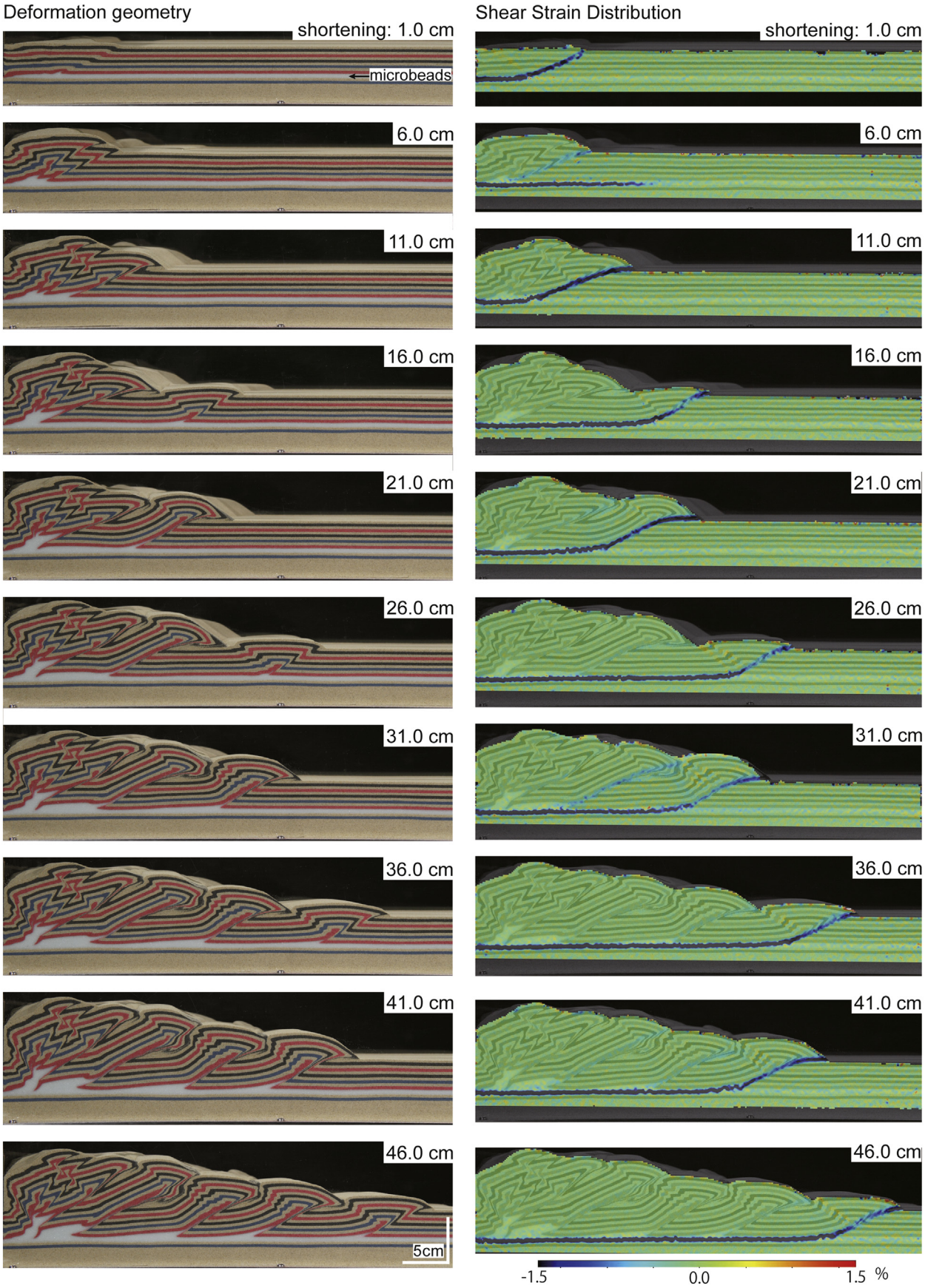

Figure 4. Results of the analog experiment, showing deformation geometry at every 5.0 cm step of horizontal shortening and shear strain distributions calculated with the digital image correlation (DIC) technique. The experiment produced a typical geometry of sequential thrusts accompanied by minor backthrusts, and an accretionary wedge inclined gently toward the deformation front. Reactivation of some older foreland-vergent thrusts can also be identified from the elevated shear strain. Surface gliding can be identified by the thinning of the top sand layers.

In this study, shear strain is defined as $(\varepsilon_{xy} + \varepsilon_{yx})/2$, where $\varepsilon_{xy}(\varepsilon_{yx})$ is a shear strain value that describes the gradient in x (y) deformation along the y (x) axis, and is therefore half of the total shear strain calculated for each 2.5×10^{-2} cm of shortening. The DIC results show that the model section can be divided into several coherent blocks, each of which has no internal shear strain, bounded by the faults where most of the shear strain is accommodated.

After 1.0 cm of horizontal shortening, one foreland thrust and a minor backthrust can be observed in the deformation geometry (Fig. 4). The shear strain distribution clearly shows that the distinct strain (in blue) in the model corresponds to the frontal thrust propagating from the microbead layer. The shear strain diagram also shows that the minor backthrust (in yellow) is located above the bend where the foreland thrust propagates from the horizontal microbead layer.

The section geometry after 6.0 cm of horizontal shortening shows that the frontal thrust is accompanied by several backthrusts and a hangingwall break-back thrust (Fig. 4). The DIC shear strain diagram, however, shows that the activity of these faults has mostly ceased, and almost all strain is concentrated along the horizontal microbead layer (Fig. 4). Such layer-parallel deformation cannot be identified without using the DIC technique.

The section geometry after 11.0, 16.0, 21.0 and 26.0 cm of shortening shows the sequential development of foreland thrusts that propagate upward from the horizontal microbead layer, and associated hangingwall folding (Fig. 4). The DIC strain distributions show that shear strain is concentrated in the foreland thrusts and in the deeper horizontal segments, along the microbead layer (Fig. 4). Strain along the foreland thrust is less than that on the horizontal segment where backthrust activity occurs (e.g., at 16.0 and 26.0 cm of shortening).

The section geometry after 31.0 cm of horizontal shortening can be regarded as a continuation of frontal-thrust displacement (Fig. 4). However, the DIC strain diagram shows that the second major foreland thrust from the deformation front also produced shear strain, suggesting that this fault has been reactivated (Fig. 4). The homogenous shear strain distribution along the second foreland thrust suggests that displacement along the fault is uniform during reactivation.

The section geometry and DIC strain distributions after 36.0, 41.0, and 46.0 cm of shortening show that deformation at these stages is primarily represented by displacement along the frontal thrust, with minor backthrust activity (Fig. 4).

4.2. Detailed deformation styles

Analysis using the DIC technique demonstrates that, despite the simplicity of the thrust experiment, deformation shows considerable temporal and spatial variation. Figure 5 shows such an example of variation in displacement along thrust faults at each shortening step between 38.050 cm and 38.275 cm. Development of sequential foreland-verging thrusts and their associated backthrusts is evident in the raw image, but changes in deformation geometry are not detectable (Fig. 5). However, the shear strain distribution produced using the DIC technique shows not only the detailed development of the frontal faults, but also reactivation of older thrusts (Fig. 5). For example, the DIC detects major shear strain along the horizontal detachment and the frontal thrust after 38.050 cm of shortening, while shear strain along previous thrusts is negligible. After the model was shortened a further 0.025 cm, shear strain along previous thrusts increased, particularly in the third thrust from the front (Fig. 5). At the same time, activity of hinterland-verging thrusts, such as backthrusts, also increased above the frontal and second foreland-verging thrusts. These results show that previous faults, including both foreland- and hinterland-verging thrusts, were reactivated simultaneously. The DIC also shows lower shear strain along the horizontal detachment below the second and third foreland-verging thrusts at this level of horizontal shortening (Fig. 5). Reactivation of previous thrusts was significantly reduced with a further 0.025 cm of shortening (38.100 cm total shortening), and the shear strain distribution closely approximates that observed before the reactivation event (after 38.050 cm; Fig. 5). Further examples of short-lived reactivation of older thrusts were observed after shortening of 38.125, 38.175, and 38.250 cm. All of these reactivated thrusts became inactive after the model was shortened by a further 0.025 cm (Fig. 5).

5. Results of numerical simulations

5.1. Deformation geometry, velocity, and interaction forces

The simulations produced a typical wedge geometry, with a series of thrust faults propagating upward from the basal detachment layer (Fig. 6). At the deformation front, the foreland-vergent thrust was accompanied by a backthrust, forming a pop-up structure. However, activity on the backthrust ceased at an early stage, and only the foreland-vergent thrust continued to develop (Fig. 6). The remnants of backthrusts can be recognized by the asymmetric pop-up structures at the front of the thrust sheets. Surface gliding was also observed at each of the foreland-dipping surfaces adjacent to the frontal thrust, producing a thinning of the upper blue (in the web version) particles, and deposition of sediments from failure at the foot of the slope (Fig. 6).

The velocity vectors, using the fixed base as a reference, show temporal and spatial variability throughout the evolution of the prism (Fig. 6). These vectors are calculated for a 0.09 cm displacement of the moving wall, and can be regarded as instantaneous values. Similar to the DIC velocity, temporal variations in faulting can be examined in detail from the velocity vectors. For example, a pop-up structure is actively formed at a very early stage in the simulation (after 90 m of horizontal shortening), but such a minor structure cannot be recognized in the deformation geometry (Fig. 6). After 2250 m of shortening, displacement occurs along the frontal thrust, accompanied by the development of a foreland-verging thrust and backthrust pair in the 'undeformed region' (Fig. 6). Such backthrusting in the undeformed region can also be found after 9000 m of shortening. Large velocity anomalies were observed in the deeper part of the prism and on the slope of the deformation front in every stage, but these were instantaneous phenomena that disappeared immediately.

The contact force diagrams show the variation in stress distributions during shortening (Fig. 6). The direction of the maximum contact force is generally sub-horizontal or slightly inclined toward the deep part of the prism, but is vertical at the shallowest part of the anticline crests. Therefore, the stress field is different in the shallow (extensional) and deep (compressional) areas of the prism. The direction and magnitude of the contact force show temporal variations during shortening, but are of much lower magnitude than the velocity vectors. In particular, deeper segments of the faults are generally subject to strong horizontal compressive forces, and little variation is evident. The compressive force reaches 2.0–4.0 km from the deformation front, despite no visible deformation occurring in this area.

5.2. Short-timescale deformation

To examine the temporal and spatial variations in velocity and contact forces, short-timescale deformation was analyzed in detail

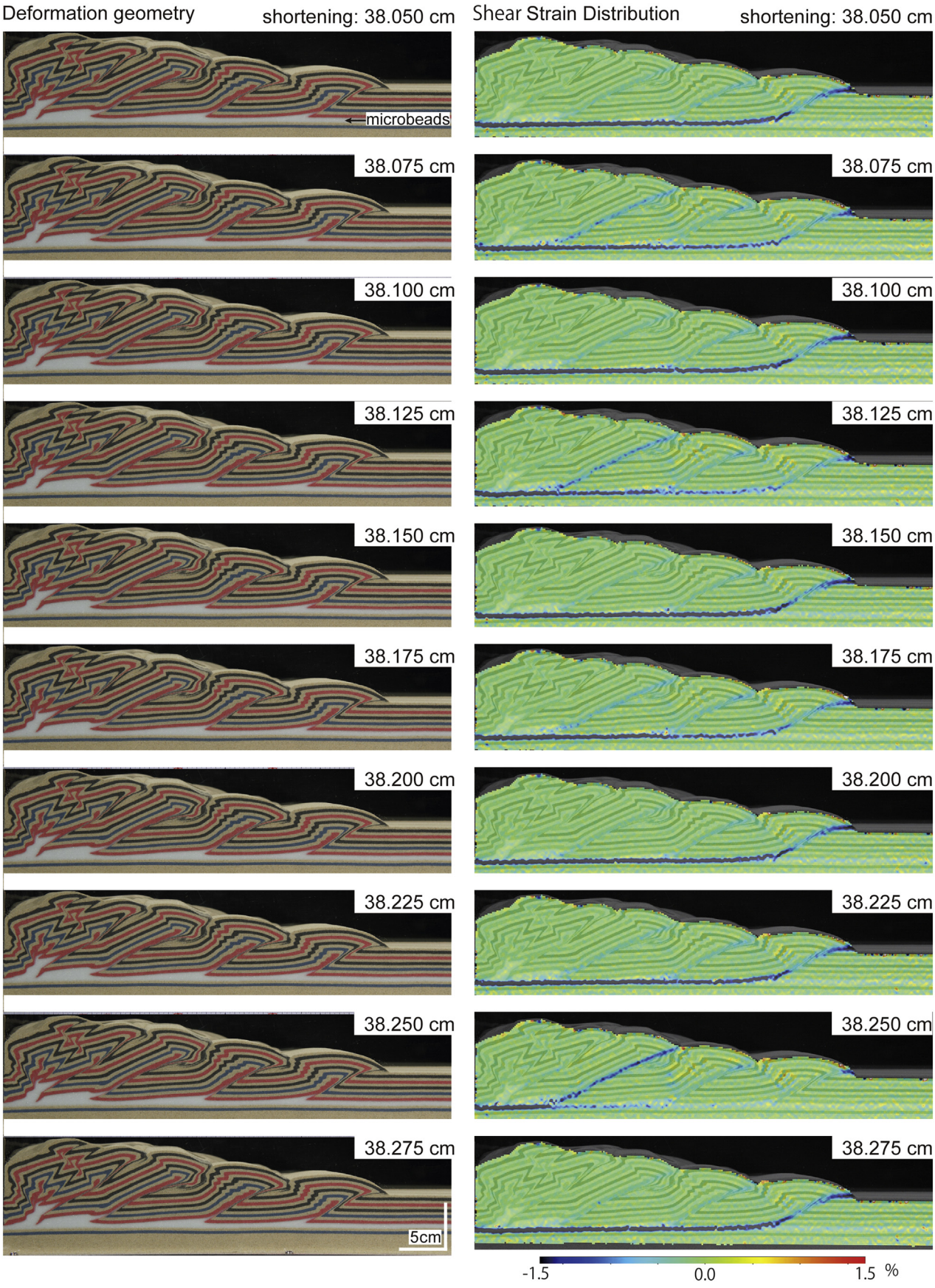

Figure 5. Detailed deformation from the analog experiment, showing deformation geometry at every 0.025 cm step of horizontal shortening, and shear strain distributions calculated with the DIC technique. The shear strain (displacement) along the frontal thrust and the horizontal detachment is a feature evident in most of the steps. The DIC analysis also reveals reactivation of older frontal thrusts, corresponding to the shear strain (color change) along the fault. The frontal thrust was continuously active but inactive at 38.125 cm and 38.250 cm of shortening. Previously formed foreland-verging thrusts showed clear evidence of reactivation at these stages, but the activity was episodic.

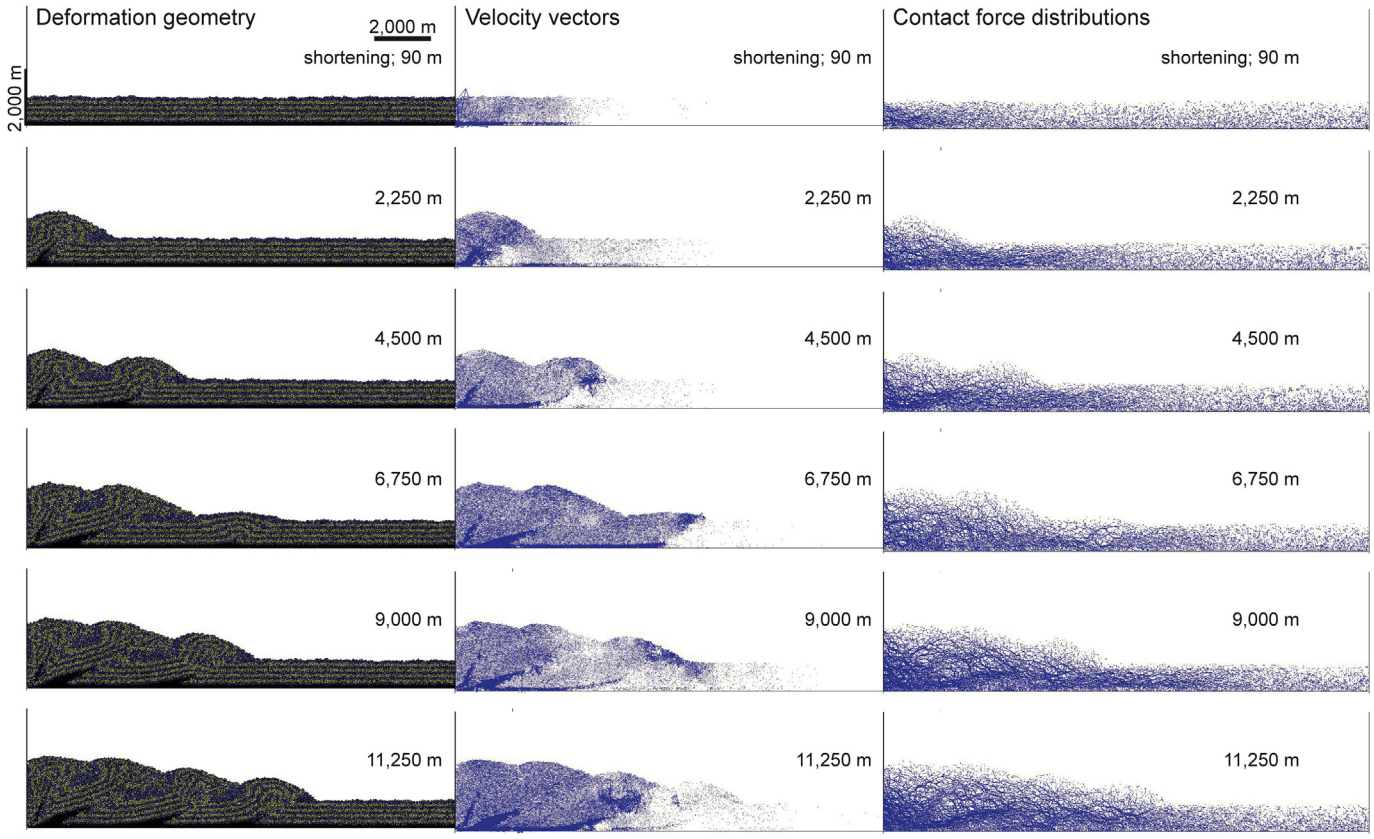

Figure 6. Results of the numerical simulation, showing deformation geometry for every 2250 m step of horizontal shortening, instantaneous velocity vectors at these steps, and contact force distributions between the particles. The simulations not only produced a typical wedge geometry with a series of thrust faults, but also showed slope failures at the prism slope, which resulted in thickness changes in the top layer. The velocity vectors use the fixed base as a reference, and are calculated for a 0.09 cm displacement of the moving wall. The vectors detect the initiation of pop-up structures in the undeformed region after 90 m and 9000 m of horizontal shortening, respectively. Large velocity anomalies can also be observed in the hangingwall of the frontal thrust, and on the slope of the deformation front. The interaction force diagrams show that the direction of the maximum contact forces is generally sub-horizontal or toward the lower right of the prism, but are vertical (i.e., extensional) at the crests of the anticlines. The compressive force extends to 2.0–4.0 km from the deformation front.

(Fig. 7). The deformation geometry showed no clear change with each 0.9 m of horizontal shortening, other than subtle displacement of the frontal thrust (Fig. 7). The velocity vectors, however, illustrate the complex nature of fault activity (Fig. 7). The frontal thrust was active after 11,162.7 m of shortening, but the activity on the lower part of the thrust ceased after a further 0.9 m of shortening (i.e., at 11,163.6 m). The upper part of the thrust is identified by a velocity anomaly that is indicative of a faulting event, and this anomaly was not apparent at the next step (11,164.5 m). This faulting event propagated upward by shortcutting the hangingwall. The disturbance observed in the hangingwall of the shortcut fault may correspond to backthrusting. At the next step (11,165.4 m), the frontal thrust was active along its entire length but the displacement was not uniform, as identified by a gradual change in velocity. A previous thrust was associated with an anomalous velocity pattern in the deeper part of this fault, suggesting reactivation. Displacement along this fault ceased in the next calculation step (i.e., 11,166.3 m).

Surface gliding is another feature that can be observed, even in such short-timescale diagrams (Fig. 7). A thin layer of 3–4 particles at the slope of the deformation front can be seen gliding down toward the foot of the slope. This gliding continued throughout the analysis, but the velocities of the surface particles show temporal and spatial variations.

The contact force diagrams show that the stress distributions in the particle assemblage are not significantly affected by fault activity (Fig. 7). The overall direction of the maximum compressional force is generally horizontal or gently inclined toward the deep part of the prism, from the moving wall toward the fixed base. The uppermost particles show a subtle variation in contact force during shortening.

6. Discussion

6.1. Temporal variations in faulting and stresses

Results of both the analog experiments and numerical simulations show that faulting has spatial and temporal variations due to cycles of lock-up and reactivation. The analog experiments revealed that the activity of the frontal thrust significantly decreased during the initiation of a new frontal pop-up structure. The fault activity completely ceased (lock-up) for a relatively short time around 6.150, 14.275, 23.900, 32.750, and 42.675 cm of shortening, corresponding to the steps at which new structures were initiated. Only the new faults were active for a short time afterward, then older thrusts experienced minor, but frequent, episodic reactivations. Shortening of 0.025 cm in the model was equivalent to 6–12 m in the natural setting. Based on the convergence rate estimated by Seno et al. (1993), this corresponds to plate convergence over 150–300 years. Therefore, the fault reactivations observed in the analog models suggest that episodic reactivations of fault activity in the Nankai accretionary prism occur over timescales of hundreds of

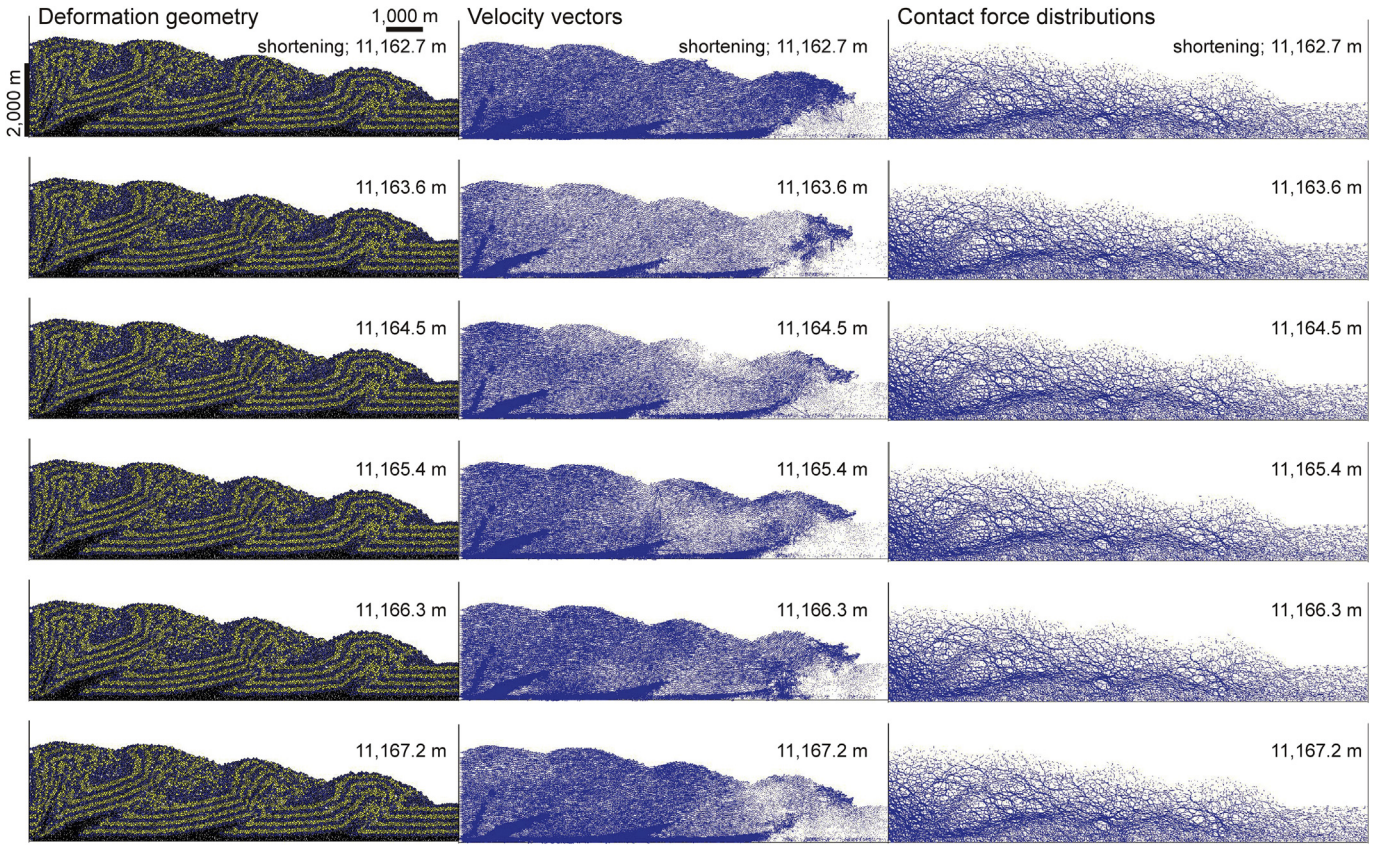

Figure 7. Short-timescale deformations observed in the numerical simulation, showing deformation geometry, velocity vectors, and contact force distributions for each 0.9 m of horizontal shortening. The deformation geometry shows no clear change, but the velocity vectors reveal reactivation of the frontal thrust. The frontal thrust was active after 11,162.7 m of shortening, but the activity on the lower part of the thrust ceased at 11,163.6 m. The upper part of the thrust contains a velocity anomaly that is indicative of faulting; this anomaly disappeared at the next step (11,164.5 m). The frontal thrust was active along almost its entire length during the next step (11,165.4 m), although the displacement along thrust was not uniform. Surface gliding continued throughout the simulation, moving a few particles at the slope of the deformation front. The contact force diagrams show that the overall direction of maximum compressional force is generally toward the lower right, and is not significantly affected by fault activity.

years. Activity on the reactivated fault continued until a new frontal structure was initiated. Reactivation of pre-existing fault systems is therefore common, except during the period after initiation of a new frontal structure. Adam et al. (2005) reported similar fault reactivations in their analog experiments, showing that such reactivation happens when the frontal thrust has locked up. That is, reactivation in their models occurred for a shorter time than that in the present study. This difference may be a result of differences in the configuration of the models used. We inserted a microbead layer as the detachment layer, and this low-friction material was generally distributed along each fault surface as a result of fault displacement. This is because the lower part of the fault surfaces initiated as a part of the detachment fault within the microbead layer, and the material immediately above this part of the faults was entirely formed of these microbeads. These thin microbead layers may have reduced the friction along the faults and made reactivation easier. This is analogous to natural examples where faults maintain reduced friction for a relatively long time. Adam et al. (2005) used homogenous material, and used the top surface of the base plate of their apparatus as the detachment. This may correspond to natural examples where friction of the sequential foreland-verging thrusts is reduced significantly from initial values over a relatively short timescale.

The numerical simulations suggest that fault activity in an accretionary prism is complex during deformation over a short timescale. Displacement along the frontal thrust only occurs on parts of the fault surface, and is commonly episodic due to cycles of lock-up and reactivation. This may be closely related to frictional stick–slip behavior during faulting, similar to that described by Yamada et al. (2006a). As the shortening intervals of 0.9 m presented in this paper correspond to plate convergence over a few decades (based on the convergence rate estimated by Seno et al. (1993)), the simulation suggests such complex heterogeneity may also be observed in natural fault activity over an equally brief timescale.

In contrast, the stress field in the simulation seems to be relatively stable within the thrust sheets, even around faults during periods of lock-up. Such stable stress fields were also reported at the fault that caused the earthquake in the Kobe area, western Japan, in 1995. Stress-measurement experiments conducted at boreholes drilled through the fault surface revealed that the stress field recovered to its pre-earthquake state after 5 years (Tadokoro and Ando, 2002). Returning to the present study, temporal variations in the stress field may be more significant in the shallow regions where hangingwall anticlines are developing. The contact force diagrams show that the magnitude of the force is minor, and the direction is perpendicular to the surface at the crest of the anticlines (Figs. 6 and 7). This is presumably due to the effects of outer-arc extension, which reduces lateral compression. Such stress states in anticlines may frequently fluctuate through the episodic development of folds, caused by cyclic displacement of the underlying thrust and topographic effects that result in surface gliding.

6.2. Surface gliding

The analog experiments showed that the activity of the frontal thrust generated surface gliding on the adjacent foreland-dipping surface. Deposits from slope failure are generally sheared during the gliding process, and therefore usually exhibit higher porosity than undisturbed sediments. Given that they are captured in the accretionary prism by the displacement of the frontal thrust and by backthrusts of consequent foreland-verging frontal thrusts in the later stages, their distribution may play an import role in controlling fluid flow in accretionary prisms. Yamada et al. (2010, 2012) conducted analog shortening experiments and reported that surface gliding is active over the area that the underlying thrust displaces. This study shows that pre-existing thrust systems also reactivate; thus, surface gliding could also occur along slopes above such reactivated faults. The dip of the slopes is generally gentler than that associated with the frontal thrust, due to rotation of the hangingwall by frontal-thrust displacement. The potential to cause surface gliding is therefore lower than that for the slope above the frontal thrust.

The numerical simulations showed that activity of the frontal thrust is unclear at its shallowest part, due to disturbance from surface gliding. As noted in the analog experiments, this surface gliding is only seen at the foreland-dipping surface adjacent to the thrust, and may be triggered by thrust activity in the near-surface area. The lack of a clear discontinuity at the base of such surface gliding, and the gradual change in the velocity vectors of the surface particles, suggest that the gliding body is sheared as a whole, and includes a number of microscale shear planes.

6.3. Dilation along faults in models

The materials used in this study exhibit dilation along shear planes. Yamada et al. (2006b) conducted a series of shear-box (2 cm height) tests and reported that the Toyoura sand and microbeads showed 0.2–0.6% (0.04–0.12 mm) and 0.15–0.30% (0.03–0.06 mm) porosity (height) increase, respectively. The materials were sifted in both the box tests and analog experiments, meaning that they may show similar deformation behaviors. The particles in the simulation models also experienced dilation during shearing. Miyakawa et al. (2006) conducted 3D DEM simulations to produce simple accretionary wedges, and measured the bulk porosity of serially produced cubes in the numerical models. The porosity of thrust surfaces in the model increased by 5–10% from the intact state, and permeability increased by 20–100%. Such dilatational characteristics of the materials agree with the strain-softening behavior observed during the shearing tests, and may favor reactivation of the thrusts.

6.4. Implications for fluid flow within prisms

The results of modeling showed that the frontal thrust is generally active. As the frontal thrust is generated by branching from the décollement, this implies that formation fluids can generally migrate from depth to the frontal thrust along the décollement surface. Such fluid migration to the frontal thrust has been reported by heat-flow studies in natural accretionary prisms, as higher temperature fluids are present at greater depths due to the geothermal gradient. Ashi et al. (2002) reported that heat flow, estimated from BSR depth, increases toward the trench in the western Nankai area. A trenchward increase in heat flow has also been reported in Barbados (Ferguson et al., 1993), the Cascadia Margin (Hyndman et al., 1993), and Sulawesi (Delisle et al., 1998), suggesting that migration of warm fluids from depth to the frontal thrusts is a common process in accretionary prisms. Fluid migration from depth has also been reported at ODP site 808 near the toe of the Nankai prism off Muroto, where transport of exotic pore waters from depth has been confirmed by down-hole mineralogy, isotopic ratios, and chloride concentrations (Kastner et al., 1993; Underwood et al., 1993). Rowe et al. (2012) employed coupled numerical methods of deformation and fluid flow, and argued that excess pore pressure beneath the frontal thrust plays a significant role in defining the location of deformation. Even though the models presented in this paper do not include the effects of pore pressure, the frontal thrusts are generally accompanied by deposits related to surface gliding in the footwall. These deposits are likely to have higher porosity than the surrounding prism body, and could behave as weaker sediments in the presence of elevated fluid pressure.

The results of modeling also showed that older thrusts are commonly reactivated, which suggests that formation fluids may move along older, weaker structures. This is consistent with the BSR pattern at Hydrate Ridge, off Oregon, and Makran margin, off

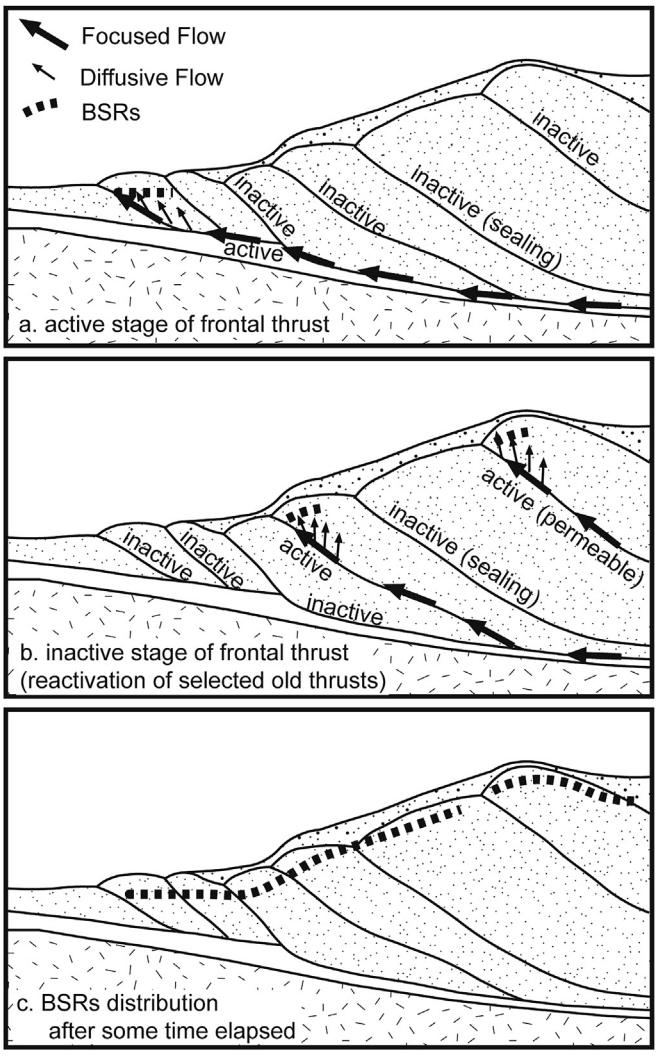

Figure 8. Revised fluid flow model based on the results of modeling during this study. (a) Fluid flow in accretionary prisms is generally focused along the frontal thrust at depth before undergoing shallower diffusive flow into the surrounding permeable sediments. (b) Periods of inactivity of the frontal thrust may be associated with the reactivation of existing thrusts; these reactivated thrusts can then act as fluid pathways. (c) Iterations of these stages contribute to form the overall distribution of BSRs over a long period of time (cf. Fig. 1).

Pakistan, where BSRs tend to be shallow and adjacent to thrust faults in the prism sediments (Minshull and White, 1989; Zwart et al., 1996). Such localized and shallow BSRs strongly suggest that anomalous warm fluid migrates along thrust surfaces.

Temporal and spatial variations in faulting and in the stress field during prism development, observed in both the analog and numerical models, suggest that fluctuations in fluid flow may be controlled by these variations. Episodic faulting and reactivation of pre-existing thrusts suggest that focused fluid flow along fault surfaces is also episodic.

The internal stress field causes significant fluctuations in inter-granular permeability. Results of the numerical simulations suggest that the stress field at depth is characterized by strong horizontal compression, and is relatively stable. In the shallower segment, however, the stress field causes horizontal extension and shows more frequent variability. This suggests that fluid flow is relatively stable in the deeper segment of the prism, but fluctuates in the shallower segment.

Fig. 8 shows our revised fluid flow model based on the modeling undertaken during this study. Fluid flow in accretionary prisms may generally be focused along the décollement and the frontal thrust, as these faults are frequently active (Fig. 8a). In comparison, fluids within the shallow part of the prism migrate further into the surrounding permeable sediments by diffusive flow (Fig. 8a). The non-uniform displacement of the frontal thrust, identified in the numerical simulations described above, suggests that the frontal thrust may be partly sealed in certain areas, contributing to diffusive flow within the surrounding sediments. Inactive parts of the frontal thrust may cause deeply sourced fluids to use other reactivated faults as pathways before then migrating into the surrounding sediments (Fig. 8b). Such variation in fluid flow may contribute to the long-time formation of widely distributed BSRs within accretionary prisms (Fig. 8c).

6.5. Implications for episodic transport of economic hydrocarbons within thrust belts

The fluid flow model presented here is applicable to hydrocarbon migration within fold-and-thrust belts, primarily as the tectonic environment of these belts is similar to that of accretionary prisms. Our model suggests that formation fluids generally migrate from depth to the frontal thrust through the basal detachment surface, with temporal and spatial variations caused by fluctuations in faulting and stress fields. Episodic reactivation of older thrusts within the models presented here indicates that formation fluids may episodically shortcut along older structures within these thrust belts. This means that internal stress-field-controlled fluid flow through inter-granular pore spaces is likely to be relatively stable at depth, but will fluctuate in shallower regions.

6.6. Effects of particle size

This study approximates the geologic body as an assemblage of particles, the diameters of which would be several meters when scaled to the actual size of the Nankai prism. At a 1:1 scale, the grains of sand and microbeads used in the experiments would be 8–15 and 2–4 m, respectively, while the size of particle-A and particle-B in the simulations corresponds to 12–30 and 6–10 m, respectively. Although such large particle sizes are not equivalent to those of the natural setting, previous use of 'sandbox' experiments, and their application to natural structures, suggests that this approximation is valid. The particle size, however, may affect the model results, especially the magnitude of internal forces. Given that forces propagate through the contact points of each particle, contact force tends to concentrate in larger particles, meaning that the magnitude of forces recorded may be controlled by particle size. The contact force diagrams derived from the numerical model suggest that the force above the basal detachment layer is greater than the force in the basal layer (Figs. 6 and 7). The magnitude of the contact forces may be reduced by the smaller size (i.e., increased number) of particles in the detachment layer, if the layer thickness of the detachment is constant.

The particle size may not significantly affect the velocity distributions in the analog and numerical modeling presented in this paper. As described earlier, the DIC results obtained from the analog experiments indicate that the model section can be divided into several coherent blocks, with each block having no internal shear strain. That means that the particles do not displace independently but behave as part of a larger block, indicating that velocity differences between two adjacent blocks are independent of the size of the particles involved. We admit that the particle size influences the width of faults, as shear zones within loose granular materials are generally a few particles thick (e.g., Mandl et al., 1977). This indicates that shear strain values determined by velocity differences (relative displacement between the two adjacent blocks) and fault widths are affected by changes in particle size. It is because of this variation with particle size that we have focused on the qualitative distribution of strain, rather than discussing strain values in detail.

6.7. Physical implications of particle models

The particle models show that deformation of a natural geologic body can be modeled by a combination of the rotation of virtual rigid bodies of a few meters diameter, and slip at the boundaries of virtual rigid bodies.

Natural geology generally includes a significant number of faults, and the overall style of deformation produced by the faults may be represented by displacement in a number of smaller faults over a short distance. These faults act as boundaries, delineating blocks that can be considered rigid when modeling mesoscale deformation. Natural folding can also be modeled by using the sum of minor slip motions at the boundaries between the virtual bodies in a model. This is made possible by recent advancements in simulation technology for fluid dynamics, including LBM (Lattice Boltzmann Method; e.g., Succi (2001)), in which a fluid is modeled as an assemblage of virtual particles. This method also allows particle flow in models to approximate natural fluid flow.

7. Conclusions

The mechanism for the accumulation of methane hydrates at the Nankai prism is strongly controlled by the migration pathways of formation fluid along faults and through inter-granular pore spaces. This study examined these processes using analog and numerical models, and the results suggest that fluid flow along fault surfaces may be discontinuous, but formation fluids generally migrate to the deformation front. Pre-existing faults can also be conduits for transporting formation fluids from depth, except during periods where the frontal thrust is actively developing. Inter-granular permeability may fluctuate due to variations in the internal stress field, but fluid flow is likely to be stable in the deeper segment of the prism. This research proposes a model for the dynamic nature of prism deformation and fluid flow, which provides fundamental knowledge that can be used to explore methane hydrates at convergent margins. This model can also be applied to hydrocarbon migration in fold-and-thrust belts.

Acknowledgments

We acknowledge grants funded by the Japan Oil Gas Metal Exploration Corporation (JOGMEC) and Japan Petroleum Exploration (JAPEX). JOGMEC and JAPEX granted permission to publish this work. We also acknowledge a Grant-in-Aid for Scientific Research (KAKENHI: 213101115) and a Grant-in-Aid for Scientific Research on Innovative Areas (21107002). An earlier version of this manuscript was significantly improved by comments from John Suppe, Fabrizio Storti, and Jose de Vera, and the authors acknowledge their constructive criticism. We also thank two anonymous reviewers and Associate Editor Adam Bumby for constructive comments that improved the manuscript. Hiroto Nakagiri and Masashi Nakatsukasa helped with the experiments and the DIC analysis; the ring shear testing was conducted with the cooperation with Juergen Adam.

References

Adam, J., Urai, J.L., Wieneke, B., Oncken, O., Pfeiffer, K., Kukowski, N., Lohrmann, J., Hoth, S., van der Zee, W., Schmatz, J., 2005. Shear localisation and strain distribution during tectonic faulting — new insights from granular-flow experiments and high-resolution optical image correlation techniques. J. Struct. Geol. 27, 283–301.

Allison, E., Boswell, R., 2007. Methane Hydrate: Future Energy Within Our Grasp. Office of Fossil Energy and National Energy Technology Laboratory. Available online: http://www.fossil.energy.gov/programs/oilgas/publications/methane_hydrates/MHydrate_overview_06-2007.pdf.

Ando, M., 1975. Source mechanisms and tectonic significance of historical earthquakes along the Nankai Trough, Japan. Tectonophysics 27, 119–140.

Aoki, Y., Tamano, T., Kato, S., 1983. Detailed structure of the Nankai Trough from migrated seismic sections. Am. Assoc. Petrol. Geol. Mem. 34, 309–322.

Ashi, J., Tokuyama, H., Taira, A., 2002. Distribution of methane hydrate BSRs and its implication for the prism growth in the Nankai Trough. Mar. Geol. 187, 177–191.

Baba, K., Yamada, Y., 2004. BSRs and associated reflections as an indicator of gas hydrate and free gas accumulation — an example of accretionary prism and forearc basin system along the Nankai Trough, off central Japan. Resour. Geol. 54, 11–24.

Bangs, N.L.B., Shipley, T.H., Moore, G.F., Gulick, S.P.S., Nakamura, Y., 2004. Evolution of the Nankai trough décollement from the trench into the seismogenic zone: inferences from 3-D seismic reflection imaging. Geology 32, 273–276.

Bangs, N.L., Musgrave, R.J., Tréhu, A.M., 2005. Upward shifts in the south Hydrate Ridge gas hydrate stability zone following post-glacial warming offshore Oregon. J. Geophys. Res. 110, B03102. http://dx.doi.org/10.1029/2004JB003293.

Barton, C.A., Zoback, M.D., Moos, D., 1995. Fluid flow along potentially active faults in crystalline rock. Geology 23, 683–686.

Byerlee, J.D., 1993. Model for episodic flow of high-pressure water in fault zones before earthquakes. Geology 21, 303–306.

Claypool, G.E., Kaplan, I.R., 1974. The origin and distribution of methane in marine sediments. In: Kaplan, I.R. (Ed.), Natural Gases in Marine Sediments. Plenum, New York, pp. 99–139.

Clennell, M.B., Henry, P., Hovland, M., Booth, J.S., Winters, W.J., Thomas, M., 2000. Formation of natural gas hydrates in marine sediments: gas hydrate growth and stability conditioned by host sediment properties. Ann. N. Y. Acad. Sci. 912, 887–896.

Cobbold, P.R., Castro, L., 1999. Fluid pressure and effective stress in sandbox models. Tectonophysics 301, 1–19.

Cobbold, P.R., Durand, S., Mourgues, R., 2001. Sandbox modelling of thrust wedges with fluid-assisted detachments. Tectonophysics 334, 245–258.

Collett, T.S., 2002. Energy resource potential of natural gas hydrates. Am. Assoc. Petrol. Geol. Bull. 86, 1971–1992.

Colletta, B., Bale, P., Ballard, J.F., Letouzey, J., Pinedo, R., 1991. Computerized X-ray tomography analysis of sandbox models: examples of thin-skinned thrust systems. Geology 19, 1063–1067.

Cundall, P.A., Strack, O.D.L., 1979. A discrete numerical model for granular assemblies. Geotechnique 29, 47–65.

Davie, M.K., Buffett, B.A., 2001. A numerical model for the formation of gas hydrate below the seafloor. J. Geophys. Res. 106, 495–514.

Davis, E.E., Hyndman, R.D., Villinger, H., 1990. Rates of fluid expulsion across the northern Cascadia accretionary prism: constraints from new heat flow and multichannel seismic reflection data. J. Geophys. Res. 95, 8869–8890.

Delisle, G., Beiersdorf, H., Neben, S., Steinmann, D., 1998. The geothermal field of the North Sulawesi accretionary wedge and a model on BSR migration in unstable depositional environments. In: Henriet, J.-P., Mienert, J. (Eds.), Gas Hydrates: Relevance to World Margin Stability and Climatic Change, Geological Society of London Special Publication, vol. 137, pp. 267–274.

Donze, F., Mora, P., Magnier, S., 1994. Numerical simulation of faults and shear zones. Geophys. J. Int. 116, 46–52.

Dugan, B., Flemings, P.B., 2000. Overpressure and fluid flow in the new jersey continental slope: implications for slope failure and cold seeps. Science 289, 288–291.

Dvorkin, J., Helgerud, M.B., Waite, W.F., Kirby, S.H., Nur, A., 2000. Introduction to physical properties and elasticity models. In: Max, M. (Ed.), Natural Gas Hydrates in Oceanic and Permafrost Environments. Springer, New York, pp. 245–460.

Expedition 311 Scientists, 2005. Cascadia margin gas hydrates. IODP Prel. Rept. 311. http://dx.doi.org/10.2204/iodp.pr.311.

Ferguson, I.J., Westbrook, G.K., Langseth, M.G., Thomas, G.P., 1993. Heat flow and thermal models of the Barbados Ridge accretionary complex. J. Geophys. Res. 98, 4121–4142.

Finch, E., Hardy, S., Gawthorpe, R., 2003. Discrete element modelling of contractional fault-propagation folding above rigid basement fault blocks. J. Struct. Geol. 25, 515–528.

Finkbeiner, T., Barton, C.A., Zoback, M.D., 1997. Relationships among in-situ stress, fractures and faults, and fluid flow: Monterey Formation, Santa Maria Basin, California. Am. Assoc. Petrol. Geol. Bull. 81, 1975–1999.

Fujii, T., Saeki, T., Kobayashi, T., Inamori, T., Hayashi, M., Takano, O., Takayama, O., Kawasaki, T., Nagakubo, S., Nakamizu, M., Yokoi, K., 2008. Resource assessment of methane hydrate in the eastern Nankai Trough, Japan. In: Proceedings of 2008 Offshore Technology Conference. Houston, Texas, U.S.A. (OTC19310).

Graveleau, F., Malavieille, J., Dominguez, S., 2012. Experimental modelling of orogenic wedges: a review. Tectonophysics 538–540, 1–66.

Gutscher, M., Kukowski, N., Malavieille, J., Lallemand, S., 1996. Cyclical behavior of thrust wedges: insights from high basal friction sandbox experiments. Geology 24, 135–138.

Henry, P., Lallemant, S.J., Nakamura, K., Tsunogai, U., Mazzotti, S., Kobayashi, K., 2002. Surface expression of fluid venting at the toe of the Nankai wedge and implications for flow paths. Mar. Geol. 187, 119–143.

Hickman, S., Sibson, R., Bruhn, R., 1995. Introduction to special section: mechanical involvement of fluid in faulting. J. Geophys. Res. 100, 12831–12840.

Hryciw, R.D., Raschke, S.A., Ghalib, A.M., Horner, D.A., Peters, J.F., 1996. Video tracking for experimental validation of discrete element simulation of large discontinuous deformations. Comput. Geotech. 21, 235–253.

Hubbert, M.K., 1937. Theory of scaled models as applied to the study of geological structures. Bull. Geol. Soc. Am. 48, 1459–1520.

Hyndman, R.D., Davis, E.E., 1992. A mechanism for the formation of methane hydrate and sea floor bottom simulating reflectors by vertical fluid expulsion. J. Geophys. Res. 97, 7025–7041.

Hyndman, R.D., Wang, K., Yuan, T., Spence, G.D., 1993. Tectonic sediment thickening, fluid expulsion, and the thermal regime of subduction zone accretionary prisms: the Cascadia margin off Vancouver Island. J. Geophys. Res. 98, 21865–21876.

Hyndman, R.D., Wang, K., Yamano, M., 1995. Thermal constraints on the seismogenic portion of the southwestern Japan subduction thrust. J. Geophys. Res. 100, 15373–15392.

Japan National Oil Corporation (JNOC), 1998. In: Proceedings of International Symposium on Methane Hydrates Research in the Near Future, p. 399.

Japan Oil, Gas and Metals National Corporation (JOGMEC), 2011. Overview of the first offshore production test of methane hydrate in the Nankai Trough. Available online: http://www.jogmec.go.jp/english/information/bids/docs/2011/at4_110811_02.pdf.

Kamei, R., Hato, M., Matsuoka, T., 2005. Random heterogeneous model with bimodal velocity distribution for methane hydrate exploration. Expl. Geophys. 36, 41–49.

Kastner, M., Elderfield, H., Jenkins, W.J., Gieskes, J.M., Gamo, T., 1993. Geochemical and isotopic evidence for fluid flow in the western Nankai subduction zone, Japan. In: Proceedings of Ocean Drilling Program, Scientific Results, vol. 131, pp. 397–413.

Kinoshita, M., Tobin, H., Thu, M.K., Gaillot, P., Bourlange, S., Chang, C., Conin, M., Gulick, S., Rodriguez, M.J.J., Martin, K.M., McNeill, L., Miyakawa, A., Moore, J.C., Nakamura, Y., Saito, S., Sawyer, D.S., Tudge, J., Yamada, Y., 2008. NanTroSEIZE stage IA: NanTroSEIZE LWD transect. In: Integrated Ocean Drilling Program, Preliminary Report, vol. 314, pp. 1–63.

Koyi, H.A., Mancktelow, N.S., 2001. Tectonic Modeling: a Volume in Honor of Hans Ramberg. In: Geological Society of America Memoir, vol. 193.

Kvenvolden, K.A., McDonald, T.J., 1985. Gas Hydrates of the Middle America Trench. Deep Sea Drilling Project Leg 84, initial report, pp. 667–682.

La Vision, 2010. Product Manual for DaVis 8.0 Software. LaVision GmbH, Gottingen, Germany.

Le Pichon, X., Boulegue, J., Charvet, J., Faure, M., Kano, K., Lallemant, S., Okada, H., Rangin, C., Taira, A., Urabe, T., Uyeda, S., 1987. Nankai Trough and Zenisu ridge: a deep sea submersible survey. Earth Planet. Sci. Lett. 83, 285–299.

Liu, H., McClay, K.R., Powell, D., 1992. Physical models of thrust wedges. In: McClay, K.R. (Ed.), Thrust Tectonics. Chapman & Hall, London, pp. 71–81.

Lohrmann, J., Kukowski, N., Adam, J., Oncken, O., 2003. The impact of analog material properties on the geometry, kinematics, and dynamics of convergent sand wedges. J. Struct. Geol. 25, 1691–1711.

Lorenson, T.D., 2000. Microscopic character of marine sediment containing disseminated gas hydrate: examples from the Blake Ridge and the Middle America Trench. In: Holder, G.D., Bishnoi, P.R. (Eds.), Gas Hydrates. Ann. N. Y. Acad. Sci. 912, 189–194.

Malavieille, J., 1984. Modélisation experimentale des chevauchements imbriqués: application aux chaînes de montagnes. Bull. Soc. Géol. Fr. 7, 129–138.

Mandl, G., de Jong, L.N.J., Maltha, A., 1977. Shear zones in granular material. Rock Mech. 9, 95–144.

Matsumoto, R., 2002. Comparison of marine and permafrost gas hydrates: examples from Nankai Trough and Mackenzie Delta. In: Proceedings of the Fourth International Conference on Gas Hydrates, pp. 1–5.
Matsushima, J., 2005. Attenuation measurements from sonic waveform logs in methane hydrate-bearing sediments at the Nankai Trough exploratory well off Tokai, central Japan. Geophys. Res. Lett. 32, L03306. http://dx.doi.org/10.1029/2004GL021786.
McClay, K.R., 1990. Deformation mechanics in analog models of extensional fault systems. In: Rutter, E.H., Knipe, R.J. (Eds.), Deformation Mechanisms, Rheology and Tectonics, Geological Society of London Special Publication, vol. 54, pp. 445–454.
McClay, K.R., 2004. Thrust tectonics and hydrocarbon systems. Am. Assoc. Petrol. Geol. Mem. 82, 667.
Minshull, T., White, R., 1989. Sediment compaction and fluid migration in Makran Accretionary Prism. J. Geophys. Res. 94, 7387–7402.
Miyakawa, A., Miyoshi, T., Yamada, Y., Matsuoka, T., 2006. Numerical simulation to estimate the influence of structural deformation to fluid flow in a modeled accretionary wedge. In: Proceedings of the 8th Society of Exploration Geophysicists of Japan International Symposium, pp. 570–575.
Miyakawa, A., Yamada, Y., Matsuoka, T., 2010. Effect of increased friction along a plate boundary fault on the formation of an out-of-sequence thrust and a break in surface slope within an accretionary wedge, based on numerical simulations. Tectonophysics 484, 89–99. http://dx.doi.org/10.1016/j.tecto.2009.08.037.
Moore, J.C., 1989. Tectonics and hydrogeology of accretionary prisms: role of the decollement. J. Struct. Geol. 11, 95–106.
Moore, G.F., Shipley, T.H., Stoffa, P.L., Karig, D.E., Taira, A., Kuramoto, S., Tokuyama, H., Suyehiro, K., 1990. Structure of the Nankai Trough accretionary zone from multichannel seismic reflection data. J. Geophys. Res. 95, 8753–8765.
Moore, G.F., et al., 2001. New insights into deformation and fluid flow processes in the Nankai Trough accretionary prism: results of ocean drilling program Leg 190. Geochem. Geophys. Geosyst. 2. http://dx.doi.org/10.1029/2001GC000166.
Mulugeta, G., 1988. Modeling the geometry of Coulomb thrust wedges. J. Struct. Geol. 10, 847–859.
Mulugeta, G., Koyi, H., 1992. Episodic accretion and strain partitioning in a model sand wedge. Tectonophysics 202, 319–333.
Pecher, I.A., Ranero, C.R., von Huene, R., Minshull, T.A., Singh, S.C., 1998. The nature and distribution of bottom simulating reflectors at the Costa Rican convergent margin. Geophys. J. Int. 133, 219–229.
Priest, J.A., Best, A.I., Clayton, C.R.I., 2005. A laboratory investigation into the seismic velocities of methane gas hydrate-bearing sand. J. Geophys. Res. 110, B04102. http://dx.doi.org/10.1029/2004JB003259.
Research Consortium for Methane Hydrate Resources in Japan, 2008. Impacts of the second on-shore methane hydrate production test results on the Japanese resource development. Available online at: http://www.mh21japan.gr.jp/pdf/2nd production test (JE).pdf.
Rowe, K., Screaton, E.J., Ge, S., 2012. Coupled fluid-flow and deformation modeling of the frontal thrust region of the Kumano Basin transect, Japan: implications for fluid pressures and decollement downstepping. Geochem. Geophys. Geosyst. 13, Q0AD23. http://dx.doi.org/10.1029/2011GC00386.
Saltzer, S.D., 1993. Boundary conditions in sandbox models of crustal extension: an analysis using distinct elements. Tectonophysics 215, 349–362.
Saltzer, S.D., Pollard, D.D., 1992. Distinct element modeling of structures formed in sedimentary overburden by extensional reactivation of basement faults. Tectonics 11, 165–174.
Sample, J.C., 1996. Isotopic evidence from authigenic carbonates for rapid upward fluid flow in accretionary wedges. Geology 24, 897–900.
Schreurs, G., Buiter, S., Boutelier, D., Cavozzi, C., Corti, G., Costa, E., Cruden, A., Daniel, J.-M., DelVentisetti, C., Brady, J.E., Hoffmann-Rothe, A., Hoth, S., Koyi, H., Kukowski, N., Lohrmann, J., Mengus, J.-M., Montanari, D., Nilfouroshan, F., Ravaglia, A., Schlische, R., Withjack, M., Yamada, Y., 2006. Analog benchmarking: results of shortening and extension experiments. In: Schreurs, G., Buiter, S. (Eds.), Analog and Numerical Modelling of Crustal Scale Processes, Geological Society of London Special Publication, vol. 253, pp. 1–27.
Seno, T., Stein, S., Gripp, A.E., 1993. A model for the motion of the Philippine Sea plate consistent with NUVEL-1 and geological data. J. Geophys. Res. 98, 17941–17948.
Shipboard Scientific Party Site 1041, 1997. In: Proceedings of Ocean Drilling Program, Initial Report, vol. 170, pp. 153–188.
Sibson, R.H., 1990. Conditions of fault-valve behavior. In: Rutter, E.H., Knipe, R.J. (Eds.), Deformation Mechanisms, Rheology and Tectonics, Geological Society of London Special Publication, vol. 54, pp. 15–28.
Sibson, R.H., 1992. Implications of fault-valve behaviour for rupture nucleation and recurrence. Tectonophysics 192, 283–293.
Sleep, N.H., Blanpied, M.L., 1992. Creep, compaction and the weak rheology of major faults. Nature 359, 687–692.
Storti, F., Salvini, F., McClay, K., 1997. Fault-related folding in sandbox analogue models of thrust wedges. J. Struct. Geol. 19, 583–602.
Storti, F., Salvini, F., McClay, K., 2000. Synchronous and velocity-partitioned thrusting, and thrust polarity reversal in experimentally produced, doubly-vergent thrust wedges: implications for natural orogens. Tectonics 19, 378–396.
Strayer, L.M., Suppe, J., 2002. 3D mechanical modeling of thrust propagation: distinct-element method. J. Struct. Geol. 24, 637–650.
Succi, S., 2001. The Lattice Boltzmann Equation for Fluid Dynamics and Beyond. Oxford University Press, ISBN 0198503989.
Suess, E., Torres, M.E., Bohrmann, G., Collier, R.W., Greinert, J., Linke, P., Rehder, G., Tréhu, A., Wallmann, K., Winckler, G., Zuleger, E., 1999. Gas hydrate destabilization: enhanced dewatering, benthic material turnover and large methane plumes at the Cascadia convergent margin. Earth Planet. Sci. Lett. 170, 1–15.
Tadokoro, K., Ando, M., 2002. Evidence for rapid fault healing derived from temporal changes in S wave splitting. Geophys. Res. Lett. 29. http://dx.doi.org/10.1029/2001GL013644.
Taira, A., Katto, J., Tashiro, M., Okamura, M., Kodama, K., 1988. The Shimanto Belt in Shikoku, Japan – evolution of Cretaceous to Miocene accretionary prism. Mod. Geol. 12, 5–46.
Taira, A., Hill, I., Firth, J., Berner, U., Bruckmann, W., Byrne, T., Chabernaud, T., Fisher, A., Foucher, J.-P., Gamo, T., Gieskes, J., Hyndman, R., Karig, D., Kastner, M., Kato, Y., Lallement, S., Lu, R., Maltman, A., Moore, G., Moran, K., Olaffson, G., Owens, W., Pichering, K., Siena, F., Taylor, E., Underwood, M., Wilkinson, C., Yamano, M., Zhang, J., 1992. Sediment deformation and hydrogeology of the Nankai accretionary prism: synthesis of shipboard results of ODP Leg 131. Earth Planet. Sci. Lett. 109, 431–450.
Tanioka, Y., Satake, K., 2001. Coseismic slip distribution of the 1946 Nankai earthquake and aseismic slips caused by the earthquake. Earth Planets Space 53, 235–241.
Tréhu, A.M., Bohrmann, G., Rack, F.R., Torres, M.E., et al., 2003. In: Proceedings of Ocean Drilling Program Initial Report, vol. 204. http://dx.doi.org/10.2973/odp.proc.ir.204. College Station, TX.
Tréhu, A.M., Long, P.E., Torres, M.E., Bohrmann, G., Rack, F.R., Collett, T.S., Goldberg, D.S., Milkov, A.V., Riedel, M., Schultheiss, P., Bangs, N.L., Barr, S.R., Borowski, W.S., Claypool, G.E., Delwiche, M.E., Dickens, G.R., Gracia, E., Guerin, G., Holland, M., Johnson, J.E., Lee, Y.-J., Liu, C.-S., Su, X., Teichert, B., Tomaru, H., Manneste, M., Watanabe, M., Weinberger, J.L., 2004. Three-dimensional distribution of gas hydrate beneath southern Hydrate Ridge: constraints from ODP Leg 204. Earth Planet. Sci. Lett. 222, 845–862. http://dx.doi.org/10.1016/j.epsl.2004.03.035.
Tréhu, A.M., Ruppel, C., Holland, M., Dickens, G.D., Torres, M.E., Collet, T., Goldenberg, D., Riedel, M., Schulthesis, P., 2006. Gas hydrates in marine sediments: lessons from scientific ocean drilling. Oceanography 19, 124–144.
Tsuji, T., Matsuoka, T., Yamada, Y., Nakamura, Y., Ashi, J., Tokuyama, H., Kuramoto, S., Bangs, N.L., 2005. Initiation of plate boundary slip in the Nankai Trough off the Muroto peninsula, southwest Japan. Geophys. Res. Lett. 32, L12306.
Tsuji, Y., Ishida, H., Nakamizu, M., Matsumoto, R., Shimizu, S., 2004. Overview of the MITI Nankai Trough wells: a milestone in the evaluation of methane hydrate resources. Resour. Geol. 54, 3–10.
Ujiie, K., Hisamitsu, T., Taira, A., 2003. Deformation and fluid pressure variation during initiation and evolution of the plate boundary décollement zone in the Nankai accretionary prism. J. Geophys. Res. 108 (B8), 2398. http://dx.doi.org/10.1029/2002JB002314.
Underwood, M.B., Pickering, K., Gieskes, J.M., Kastner, M., Orr, R., 1993. Sediment geochemistry, clay mineralogy, and diagenesis: a synthesis of data from Leg 131, Nankai Trough. In: Proceedings of Ocean Drilling Program Scientific Results, vol. 131, pp. 343–363.
von Houne, R., Scholl, D.W., 1991. Observations at convergent margins concerning sediment subduction, subduction erosion, and the growth of continental crust. Rev. Geophys. 29, 279–316.
Waseda, A., 1998. Organic carbon content, bacterial methano-genesis, and accumulation process of gas hydrates in marine sediments. Geochem. J. 32, 143–157.
Wilkins, S.J., Naruk, S.J., 2007. Quantitative analysis of slip-induced dilation with application to fault seal. Am. Assoc. Petrol. Geol. Bull. 91, 97–115.
Wiprut, D., Zoback, M.D., 2000. Fault reactivation and fluid flow along a previously dormant normal fault in the northern North Sea. Geology 28, 595–598.
Wolf, H., König, D., Triantafyllidis, T., 2003. Experimental investigation of shear band patterns in granular material. J. Struct. Geol. 25, 1229–1240.
Yamada, Y., McClay, K.R., 2003a. Application of geometric models to inverted listric fault systems in sandbox experiments. 1: 2D hanging wall deformation and section restoration. J. Struct. Geol. 25, 1551–1560.
Yamada, Y., McClay, K.R., 2003b. Application of geometric models to inverted listric fault systems in sandbox experiments. 2: insights for possible along strike migration of material during 3D hanging wall deformation. J. Struct. Geol. 25, 1331–1336.
Yamada, Y., McClay, K.R., 2004. 3D analog modelling of inversion thrust structures. In: McClay, K. (Ed.), Thrust Tectonics and Hydrocarbon Systems. Am. Assoc. Petrol. Geol. Mem. 82, 276–301.
Yamada, Y., Ueda, S., Kaneda, K., Baba, K., Matsuoka, T., 2004. Analog and digital modelling of accretionary prisms with granular materials. Boll. Geofis. Teor. Appl. 45 (1), 168–170.
Yamada, Y., Okamura, H., Tamura, Y., Tsuneyama, F., 2005. Analog models of faults associated with salt doming and wrenching: application to offshore UAE. In: Sorkhabi, R., Tsuji, Y. (Eds.), Faults, Fluid Flow and Petroleum Traps. Am. Assoc. Petrol. Geol. Mem. 85, 95–106.
Yamada, Y., Baba, K., Matsuoka, T., 2006a. Analog and numerical modelling of accretionary prisms with a decollement in sediments. In: Buiter, S., Scherurs, G. (Eds.), Numerical and Analog Modelling of Crustal-Scale Processes, Geological Society of London Special Publication, vol. 253, pp. 169–183.
Yamada, Y., Kaneda, K., Matsuoka, T., 2006b. Influences of material properties on analogue model experiments of geologic structures. J. Soc. Mater. Sci. Jpn. 55, 452–457.
Yamada, Y., Yamashita, Y., Yamamoto, Y., 2010. Submarine landslides at subduction margins: insights from physical models. Tectonophysics 484, 156–167. http://dx.doi.org/10.1016/j.tecto.2009.09.007.

Yamada, Y., Oshima, Y., Matsuoka, T., 2012. Slope failures in analogue model experiments of accretionary wedges. In: Yamada, Y., et al. (Eds.), Submarine Mass Movements and Their Consequences, Advances in Natural and Technological Hazards Research Series. Springer, pp. 343–354.

Yamano, M., Uyeda, S., Aoki, Y., Shipley, T.H., 1982. Estimates of heat flow derived from gas hydrates. Geology 10, 339–343.

Yun, T.S., Francisca, F.M., Santamarina, J.C., Ruppel, C., 2005. Compressional and shear wave velocities in uncemented sediment containing gas hydrate. Geophys. Res. Lett. 32, L10609. http://dx.doi.org/10.1029/2005GL022607.

Zwart, G., Moore, J.C., Cochrane, G.R., 1996. Variations in temperature gradients identify active faults in the Oregon accretionary prism. Earth Planet. Sci. Lett. 139, 485–495.